International Journal of Solids and Structures 232 (2021) 111184

Contents lists available at ScienceDirect

International Journal of Solids and Structures

journal homepage: www.elsevier.com/locate/ijsolstr

Snap-through behaviors of a pre-deformed ribbon under midpoint loadings

Weicheng Huang [a,b], Chao Ma [c], Longhui Qin [a,*]

[a] School of Mechanical Engineering, Southeast University, Nanjing 211189, China
[b] Jiangsu Engineering Research Center of Aerospace Machinery, Southeast University, Nanjing 211189, China
[c] School of Electrical Engineering, Xi'an Jiaotong University, Xi'an 710049, China

ARTICLE INFO

Article history:
Received 30 April 2021
Received in revised form 27 July 2021
Accepted 29 July 2021
Available online 6 August 2021

Keywords:
Elastic ribbons
Buckling instability
Bifurcation
Numerical simulation

ABSTRACT

Based on the geometrically nonlinear Kirchhoff rod theory, the snap-through behaviors of an asymmetrically clamped ribbon under midpoint loadings are explored through a numerical approach. The pre-compressed elastic ribbon would experience supercritical pitchfork bifurcation and transform into multiple stable/unstable patterns when subjected to lateral end translations. With its midpoint pushed through a prescribed path and beyond a threshold, the pre-deformed ribbon will jump to other inverted equilibrium configurations, which is known as snap-through buckling. Instead of the well-established snap-through behaviors in 2D bistable beams, we observe several different snap-through processes for the elastic ribbons in a 3D scenario. Exploiting the efficiency and robustness of our developed discrete model, a systematic parameter sweep is performed to quantify the snap-through processes of elastic ribbons in different boundary conditions and categories, and the results of which could provide a fundamental understanding of structural mechanics and further motivate the designs and applications of engineered systems.

1. Introduction

Thin structures pervade nature, industry, and even everywhere in our daily lives, which mainly comprise one dimensional (1D) slender rods (tendrils, telephone cords, and hairs) and two dimensional (2D) thin plates/shells (clothes, eggshells, and leaves). Their special geometric property allows geometrically nonlinear deformations when subjected to moderate external forces or simple boundary conditions, e.g., buckling, folding, and snapping, making them suitable for the design of advanced metamaterials and intelligent systems in mechanical engineering (Hu and Burgueño, 2015; Bertoldi et al., 2017; Faris and Nayfeh, 2007). Specifically, snap-through buckling is a swift transformation process between multiple phases in response to external loadings or actuations, which could be found in both natural environments and artificial systems, such as Venus flytrap (Forterre et al., 2005), slap bracelet (Kebadze et al., 2004), toy poppers (Pandey et al., 2014), and soft robots (Chen et al., 2018; Tang et al., 2020). Tremendous investigations have been carried out focusing on the snap-through buckling of either pre-stressed or naturally curved beams under different loading or boundary conditions, e.g., midpoint loading (Camescasse et al., 2013, 2014; Yan et al., 2019), out-of-plane compression (Zhang et al., 2019; Wan et al., 2019), asymmetrical constraints (Zhao et al., xxxx; Sano and Wada, 2018; Cazzolli and Dal Corso, 2019), and contact (Chen and Hua, 2018). Other researches have paid their attentions to the viscoelastic and dynamic performances during this sudden and dramatic change (Gomez et al., 2017; Kodio et al., 2020; Liu et al., 2021). However, most of these works were restricted into a 2D circumstance such that the twist along the ribbon centerline was ignored and thus relatively simplified models were established. Recently, the snapping and bifurcation of pre-stressed 3D ribbons under stretching (Morigaki et al., 2016), twisting (Sano and Wada, 2019), and shearing (Yu and Hanna, 2019) began to be addressed, and their beautiful but complicated configurations attract increasing interests from both solid mechanics and computer graphics communities. Here, following the previous analyses (Yu and Hanna, 2019; Huang et al., 2020), this paper is aimed at exploring the mechanism of the snap-through buckling for pre-deformed narrow ribbon under midpoint loading.

The elastic ribbon considered here is a special thin structure that lies between the 1D rod (length $L \gg$ width $W \sim$ thickness t) and 2D plate ($L \sim W \gg t$), because all its three dimensions are quite different, $L \gg W \gg t$. It is straightforward to use the Kirchhoff rod

* Corresponding author.
E-mail address: lhqin@seu.edu.cn (L. Qin).

https://doi.org/10.1016/j.ijsolstr.2021.111184
0020-7683/

model to study the mechanics of narrow ribbon, and there are much prior investigations on Kirchhoff equations, e.g., Kehrbaum and Maddocks (1999), Ameline et al. (2017), Nizette and Goriely (1999), Antman and Kenney (1981) and Antman and Jordan (1975). Moreover, the deformed configurations of 1D rod-like structures of either isotropic or anisotropic cross sections can be accurately constructed via Kirchhoff equations as long as the structure is slender, i.e., $L \gg W$ (Goyal et al., 2005; Yu and Hanna, 2019; Sano and Wada, 2019). However, the 1D approach fails to capture the experimental observation for 2D structures that are no longer slender as its width and length are in the same order of magnitude, in the case of which it is necessary to develop a 2D plate approach (Huang et al., 2020). The classical ribbon model under a developable surface assumption, e.g., Sadowsky ribbon model (Sadowsky, 1930) and Wunderlich ribbon model (Wunderlich, 1962), are fundamentally different compared with anisotropic rod model, tending to produce a singular prediction at the inflection point where the bending curvature changes its direction (Huang et al., 2020). The gap between the Kirchhoff anisotropic rod model and the developable Sadowsky ribbon model can be fulfilled by a cross-section depended regularized parameter that introduces a finite stretching on the plate midsurface (Sano and Wada, 2019; Audoly and Neukirch, xxxx). Within this study, we consider an object with $L \gg W$ as well as L/W predominant than W/t, such that the naive anisotropic rod model is accurate enough to perform the geometrically nonlinear mechanics in a narrow ribbon (Yu and Hanna, 2019; Huang et al., 2020; Audoly and Neukirch, xxxx).

On the other hand, it is challenging to solve the ordinary differential equations (ODEs) derived from functional variation directly, especially when the geometric nonlinearity is involved. To overcome this issue, Finite Element Method (FEM) was developed in the computational mechanics community to investigate structural mechanics (Wood and Zienkiewicz, 1977; Bonet and Wood, 1997; Zienkiewicz and Taylor, 2005; Hughes, 2012; De Borst et al., 2012; Liu et al., 2019). Recently, thanks to the development of discrete differential geometry (DDG), painstaking trial and error process are no longer necessary in simulating the geometrically nonlinear deformation of thin elastic structures. The DDG-based approach discretizes a smooth structure into multiple nodes and edges, while preserving its key geometric features to capture the nonlinear elastic potentials (Grinspun et al., 2006). As a variant of DDG, Discrete Elastic Rods (DER) – a numerical approach to the simulation of 1D filament, has shown surprisingly excellent performance in the field of computer graphics as well as mechanical engineering (Bergou et al., 2008, 2010).

In this work, a discrete model is developed based on the previous DER algorithm to numerically investigate the snap-through buckling of pre-deformed ribbon under midpoint loading. The clamped–clamped ribbon would first deform into different patterns induced by the longitude compression, ΔL, and the transverse shear, ΔW, referring to Fig. 1, and then may experience snap-through buckling when external actuations are introduced into the system. This specific numerical setup is chosen because of two manifests: (i) the boundary conditions considered here are simple and fundamental. The bending-twisting coupling of 1D slender objects could be completely embodied when both uniaxial compression and transverse shear are introduced into the mechanical system, in contrast to the planar bistable beams that only undergo a pure bending mode (Camescasse et al., 2013, 2014; Yan et al., 2019; Zhang et al., 2019; Wan et al., 2019; Zhao et al., xxxx; Sano and Wada, 2018; Cazzolli and Dal Corso, 2019; Chen and Hua, 2018); (ii) this naive clamped–clamped boundary constraint could induce multiple stable patterns, and their (anti) symmetric snap-through behaviors may provide a fundamental

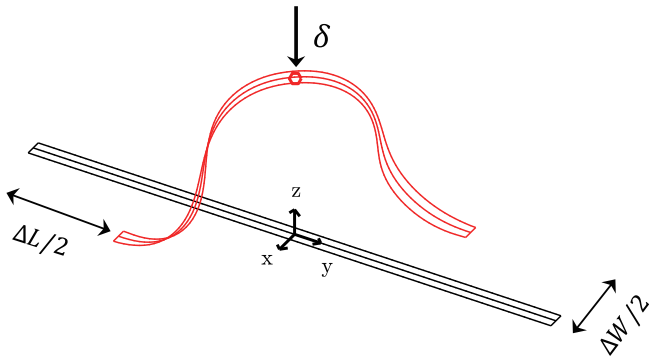

Fig. 1. Setup of numerical investigation. The pre-compressed distance is ΔL, the transverse shear is ΔW, and the midpoint displacement is denoted as δ.

understanding for some engineered systems, e.g., four-way switch and soft electronics. The behaviors for other numerical setups can be inferred and studied in a similar way. In this paper, we focus on the case that the external force is only applied onto the structural midpoint. For example, an initial planar ribbon may deform into two symmetric patterns once the uniaxial loading exceeds the threshold, known as Euler Elastica; and the structure is prone to switch to another equilibrium configuration when its midpoint (or other positions) is pushed through a prescribed path. Further, both uniaxial compression and transverse shear are introduced into the simulation model, and, therefore, the ribbon would deform into a 3D shape. As for small transverse shear, ΔW, the structure still stays as a symmetric pattern while the snap-through process between the two stable phases is similar to the well-established 2D case. Once the transverse shear surpasses a threshold, the structural symmetry cannot be maintained and four possible stable solutions may be produced. Multiple snap-through procedures can thus be observed by loading its midpoint through different prescribed trajectories. The snap-through behaviors for the four scenarios can be found in Movie S1. Finally, a systematic parameter sweep is performed on pre-compressed displacement and transverse shear to characterize the maximal actuation forces for ribbons in different configurations and various loading processes. The novel snap-through processes among the presented 4 stable configurations and 8 equilibrium patterns in the current work may inspire innovative designs of four-way switch and its related metamaterials, e.g., the total combination of permutations for the bistable metamaterial in Chen et al., 2021 can be increased from $2^{(n^2)}$ to $4^{(n^2)}$.

This paper is organized as follows. The standard Kirchhoff rod theory is reviewed first in Section 2, and then the discrete simulation for an anisotropic ribbon-like structure is formulated in Section 3. The pre-deformed patterns and snap-through buckling in elastic ribbons are presented in Section 4, followed by conclusive remarks and potential research directions in Section 5.

2. Anisotropic rod theory

A 1D ribbon can be parameterized by a space curve as its centerline, $\mathbf{r}(s)$, together with an orthonormal material frame, $\{\mathbf{m}_1(s), \mathbf{m}_2(s), \mathbf{m}_3(s)\}$, where $\mathbf{m}_3 = \mathbf{r}'$ is the tangential direction of centerline, $\mathbf{m}_1$ is the surface normal, and $\mathbf{m}_2 = \mathbf{m}_3 \times \mathbf{m}_1$ is the edge vector. The Darboux vector related to angular momentum is given by

$$\boldsymbol{\omega} = \kappa^{(1)}\mathbf{m}_1 + \kappa^{(2)}\mathbf{m}_2 + \tau\mathbf{m}_3, \tag{1}$$

where $\kappa^{(1)}$ and $\kappa^{(2)}$ are the bending curvatures while $\tau$is the twisting curvature. Assuming the bending energy along the surface normal is totally forbidden, the ribbon can only be bent along its width direction or twisted along its tangent. Thus the component of Darboux vector along the ribbon normal is absent, $\kappa^{(1)} \equiv 0$.

The balances of force, $\mathbf{N} = N_i\mathbf{m}_i$, and the momentum, $\mathbf{M} = M_i\mathbf{m}_i$ from Kirchhoff equations in the absence of distributed loads and couples are formulated by

$$\mathbf{N}\prime = \mathbf{0}, \tag{2a}$$

$$\mathbf{M}\prime + \mathbf{m}_3 \times \mathbf{N} = \mathbf{0}. \tag{2b}$$

Due to the linear constitutive relations, the components of momentum are $M_1 = EI_1\kappa^{(1)}$, $M_2 = EI_2\kappa^{(2)}$, and $M_3 = GJ\tau$, where EI_1 (and EI_2) is the bending moment of inertia and GJ is the torsional rigidity. As the cross section of the ribbon considered here is anisotropic, EI_1 performs like a Lagrange multiplier and enforces the constraint of curvature in the hard direction, $\mathbf{m}_1$. Overall, AUTO, a continuation numerical package for ODEs, can be used to derive the equilibrium configuration of elastic ribbon with prescribed boundary conditions (Doedel, 2007; Yu and Hanna, 2019).

3. Discrete model

In order to obtain the equilibrium configuration of elastic ribbons with arbitrary boundary conditions and complex loading processes, a discrete formulation – DER method – will be discussed here, which performs excellently for rod-like structures (Bergou et al., 2008, 2010).

A continuous ribbon shown schematically in Fig. 2(a) is discretized into Nnodes, $\mathbf{x}_0, \ldots, \mathbf{x}_{N-1}$, and $N-1$edge vectors, $\mathbf{e}^0, \ldots, \mathbf{e}^{N-2}$, such that $\mathbf{e}^i = \mathbf{x}_{i+1} - \mathbf{x}_i$and $i = 0, \ldots, N-2$. Hereafter, we use subscripts to denote quantities associated with the nodes, e.g., $\mathbf{x}_i$, and superscripts when associated with edges, e.g., $\mathbf{e}^i$. Each edge, $\mathbf{e}^i$, has an orthonormal adapted reference frame $\left\{\mathbf{d}_1^i, \mathbf{d}_2^i, \mathbf{t}^i\right\}$and a material frame $\{\mathbf{m}_1^i, \mathbf{m}_2^i, \mathbf{t}^i\}$, and both of them share the tangential direction, $\mathbf{t}^i = \mathbf{e}^i/|\mathbf{e}^i|$. The reference frame is updated with respect to time by a parallel transport algorithm to ensure the twist-free configuration; the material frame is related to the real structure (e.g., the surface normal vector and the edge vector of ribbon); overall, the difference between the reference frame and the material frame is defined as θ^i. Relevant descriptions can be found in Ref. Bergou et al. (2008, 2010). Node positions and twist angles constitute the $4N-1$sized degrees of freedom (DOF) vector, $\mathbf{q} = \left[\mathbf{x}_0, \theta^0, \mathbf{x}_1, \ldots, \mathbf{x}_{N-2}, \theta^{N-2}, \mathbf{x}_{N-1}\right]$, for a discrete ribbon.

The strains of a deformed ribbon comprise three parts: stretching, bending, and twisting. Firstly, the stretching strain associated with the i-th edge, $\mathbf{e}^i$, is

$$\epsilon^i = \frac{|\mathbf{e}^i|}{|\bar{\mathbf{e}}^i|} - 1, \tag{3}$$

where the notation with a bar on the top indicates the quantity evaluated in undeformed configuration. Next, referring to Fig. 2 (b), the bending strain is captured by the curvature binormal which measures the misalignment between two consecutive edges at a node $\mathbf{x}_i$,

$$(\kappa\mathbf{b})_i = \frac{2\mathbf{e}^{i-1} \times \mathbf{e}^i}{|\mathbf{e}^{i-1}||\mathbf{e}^i| + \mathbf{e}^{i-1} \cdot \mathbf{e}^i}, \tag{4}$$

and its norm is $|(\kappa\mathbf{b})_i| = 2\tan(\phi_i/2)$. The material curvatures are given by the inner products between the curvature binormal and material frame vectors,

$$\kappa_i^{(1)} = \frac{1}{2}\frac{1}{\Delta l_i}\left(\mathbf{m}_2^{i-1} + \mathbf{m}_2^i\right) \cdot (\kappa\mathbf{b})_i \tag{5a}$$

$$\kappa_i^{(2)} = -\frac{1}{2}\frac{1}{\Delta l_i}\left(\mathbf{m}_1^{i-1} + \mathbf{m}_1^i\right) \cdot (\kappa\mathbf{b})_i, \tag{5b}$$

where $\Delta l_i = (|\bar{\mathbf{e}}^i| + |\bar{\mathbf{e}}^{i-1}|)/2$ is the Voronoi length associated with the i-th node. Finally, the twisting strain at the i-th node, in the discrete setting of DER, is measured using the discrete twist

$$\tau_i = \frac{1}{\Delta l_i}\left(\theta^i - \theta^{i-1} + m_i^{\text{ref}}\right) \tag{6}$$

where m_i^{ref} is the reference twist associated with the reference frame (Bergou et al., 2008).

The total stretching, bending and twisting energies of the elastic ribbons are related to the quadratic form of strains,

$$E_s = \frac{1}{2}\sum_{i=0}^{N-2} EA\left(\varepsilon^i\right)^2 |\bar{\mathbf{e}}^i| \tag{7a}$$

$$E_b = \frac{1}{2}\sum_{i=1}^{N-2}\left[EI_1\left(\kappa_i^{(1)}\right)^2 + EI_2\left(\kappa_i^{(2)}\right)^2\right]\Delta l_i \tag{7b}$$

$$E_t = \frac{1}{2}\sum_{i=1}^{N-2} GJ(\tau_i)^2\Delta l_i. \tag{7c}$$

Notice that EA and EI_1 are much larger compared with EI_2 and GJ, such that ε^i and $\kappa_i^{(1)}$ are constrained to zero in a perfect anisotropic rod model.

The elastic forces (associated with nodal positions) and elastic moments (associated with the twist angles) are related to the gradient of total potentials,

$$\mathbf{F}^{\text{int}} = -\frac{\partial}{\partial\mathbf{q}}(E_s + E_b + E_t). \tag{8}$$

It should be noticed that the constraints (inextensibility of strip centerline and bending around $\mathbf{m}_1$ direction) are achieved through a standard Lagrange multiplier method, and the related potentials

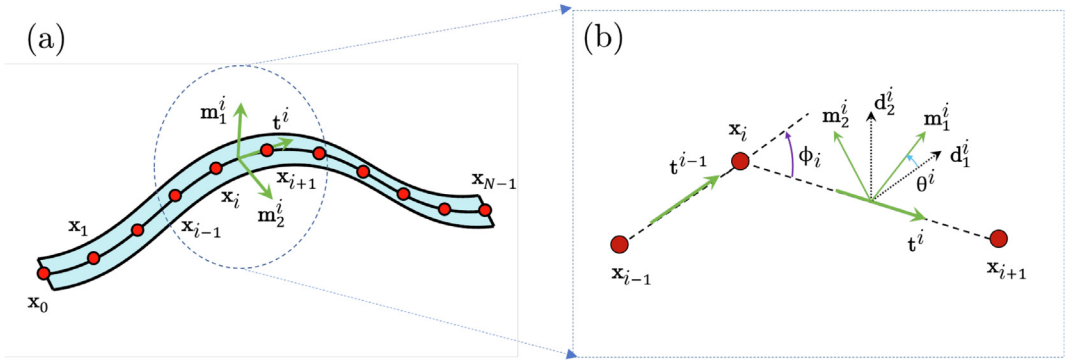

Fig. 2. (a) Discretization of a narrow ribbon. (b) Notations in discrete model.

are already included in Eq. (7), as a result of which the specific constraining forces are no longer necessary.

Overall, implicit Euler integration is used to solve the $4N-1$ sized linear system and update the DOF vector $\mathbf{q}$ and its velocity (time derivative of DOF) $\mathbf{v}=\dot{\mathbf{q}}$ from time step t_k to $t_{k+1}=t_k+h$ ($h$is the time step size):

$$\mathbf{M}\Delta\mathbf{q}_{k+1}-h\mathbf{M}\mathbf{v}_k-h^2\left(\mathbf{F}^{\text{int}}_{k+1}+\mathbf{F}^{\text{ext}}_{k+1}\right)=\mathbf{0} \tag{9a}$$

$$\mathbf{q}_{k+1}=\mathbf{q}_k+\Delta\mathbf{q}_{k+1} \tag{9b}$$

$$\mathbf{v}_{k+1}=\frac{1}{h}\Delta\mathbf{q}_{k+1}, \tag{9c}$$

where $\mathbf{F}^{\text{ext}}$ is the external force vector (e.g., gravity and damping force) and $\mathbf{M}$is the diagonal mass matrix comprised of the lumped masses. The superscript $k+1$ (and k) denotes evaluation of the quantity at time t_{k+1} (and t_k). Newton's method is used to iteratively solve the $4N-1$ sized equation of motions. Importantly, the Jacobian matrix associated with Eq. (9) is a banded matrix and the time complexity of this algorithm is $O(N)$, i.e. the computational time scales linearly with the number of nodes (Bergou et al., 2010; Jawed et al., 2014).

4. Results

In this section, the numerical results are presented based on the discrete anisotropic rod model discussed before. The supercritical pitchfork bifurcation of pre-buckled narrow ribbons under lateral transverse shear is described briefly. Then the snap-through buckling between multiple equilibrium patterns are illustrated in detail.

The physical parameters used in the current numerical investigation are as follows: ribbon length $L=300$ mm, ribbon width $W=10$ mm, ribbon thickness $t=0.5$ mm, Young's modulus $E=1$ GPa, material density $\rho=1000$ kg/m^3, and Poisson's ratio $\nu=0.2$. The Young's modulus and material density are arbitrarily choosed and have no contribution to the final static results; the Poisson's ratio has a negligible influence (Yu and Hanna, 2019; Huang et al., 2020). The ribbon centerline is divided $N=101$ nodes after a convergent study. First two nodes, last two nodes, first twisting angle, and last twisting angle, $\{\mathbf{x}_0,\theta^0,\mathbf{x}_1,\mathbf{x}_{N-2},\theta^{N-2},\mathbf{x}_{N-1}\}$, are constrained to form the clamped–clamped boundary conditions. The snap-through process will be resulted in after three steps (Fig. 1): (a) the clamped–clamped ribbon is compressed by a specified distance, ΔL, and then (b) a transverse shear, ΔW, is introduced. (c) The dirichlet boundary condition is applied to specify the position of ribbon midpoint, $\mathbf{x}_{\text{mid}}\equiv[x_{\text{mid}},y_{\text{mid}},z_{\text{mid}}]$, which will induce the snap-through process. The translation displacement is denoted by δ. The boundary nodes and midpoint are moved at an extremely low speed, $v=0.1$ mm/s, in order to avoid the inertial effect and higher order dynamic buckling modes. The boundary angles, $[\theta^0,\theta^{N-2}]$, are always fixed as zeros to ensure the twist-free state at clamped–clamped boundary conditions. It should be noted that the nondimensional quantities, $\bar{\delta}=\delta/L$, and $\bar{F}=FL^2/EI_2$, are utilized in the rest of this paper. With only the equilibrium configurations focused on (the external actuation force is computed when the structure is in equilibrium and each frame in Movie S1 is also in equilibrium condition), the damping coefficient here would be trivial.

4.1. Pre-deformed patterns of elastic ribbons

The thin ribbon would experience buckling instability when the uniaxial compressive force exceeds a threshold, known as Euler Elastica. Next, it can deform into different categories regarding the magnitude of applied transverse shear. The relations between the transverse shear and the midpoint height is quantified as shown in Fig. 3(a), with the pre-compressed displacement varying, $\Delta L/L\in\{0.2,0.3,0.4,0.5\}$. The elastic ribbon deforms to a systematic $U\pm$ (Fig. 4(a)) pattern when a small transverse shear is imposed. Regarding the nomenclature of the configurations, we follow the previous studies (Yu and Hanna, 2019; Huang et al., 2020). As the transverse shear increases and exceeds the first critical value, ΔW_1, the symmetric U pattern becomes unstable although it still stays in equilibrium. However, a supercritical pitchfork bifurcation is prone to occur and the U+ configuration would transform into either U+S+ or U+$S-$ diagram staying in a stable state, referring to Fig. 4(b) (similar for U-case). Here, with a prescribed boundary condition, there exist two stable patterns, U+S+ or U+$S-$, and one equilibrium but unstable pattern, U, known as supercritical pitchfork bifurcation (Yu and Hanna, 2019; Huang et al., 2020). A small perturbation is applied into the ribbon system to break the symmetry and induce the supercritical pitchfork bifurcation. Herein, the midpoint position is utilized to define the deformed pattern, e.g., U+S+ means both x_{mid} (or y_{mid}) and z_{mid} are positive. $\Delta W_1/L\in\{0.21,0.27,0.32,0.36\}$ are selected as the thresholds for different pre-compressed displacements. As the transverse displacement increases, U+S+ and $U-S-$ continue deformation and a $S1$ pattern is resulted in while U+$S-$ and $U-S$+ deform into the $S2$ configuration. The second threshold shear that separates the US pattern and the S pattern is where the midpoint height drops into zero and remains unchanged, shown in Figs. 3(a) and 4(c). Here, we find the second thresholds for different compressive displacements are $\Delta W_2/L\in\{0.33,0.42,0.48,0.53\}$, separately. Finally, the maximum shear for narrow ribbon (with $L\gg W$) to ensure the inextensibility of centerline is given by Eq. (10) (Yu and Hanna, 2019; Huang et al., 2020),

$$\Delta W_{\max}=\sqrt{L^2-(L-\Delta L)^2}. \tag{10}$$

A phase diagram is plotted in Fig. 3(b) to quantify the configurations of elastic ribbons under prescribed clamped boundary conditions, e.g., ΔL and ΔW. In accordance to our expectation, both two critical shear displacements, ΔW_1 and ΔW_2, and the maximum shear, $\Delta W_{\max}$, show increasing trend with respect to the compressive distance ΔL.

4.2. Snap-through buckling behaviors

With the pre-deformed elastic ribbon constructed beforehand, we now turn to the main contribution of the current study and systematically investigate the snap-through process of elastic ribbons that switches between different equilibrium configurations. Here, 4 different types of snap-through behaviors shown in Fig. 5 as well as rendered in Movie S1. Let us pay attention to the simple 2D case first. Referring to the patterns shown in Fig. 6(a1), there are two stable solutions for the pre-buckled 2D beam, and one solution can easily switch to the other one if a loading is imposed onto its midpoint. The overall procedure can be found in Fig. 6(a1)–(d1). Here, the midpoint is constrained along the z axis – the arrow in Fig. 6 – to induce the snap-through process; the external force, $\mathbf{F}\equiv[F_x,F_y,F_z]$, therefore, can be computed from the statement of force balance. It is found that the structure remains with a symmetric pattern for small vertical displacement, referring to Fig. 6b1). For a displacement larger than the critical value, a supercritical pitchfork bifurcation will occur and two possible solutions may be induced, similar to the situation discussed in the previous subsection. The external force would decrease as the midpoint's displacement increases once it exceeds the threshold value, $\bar{\delta}\approx 0.03$, referring to Fig. 7(a). Also, the external force is zero when the ribbon center reaches to the original point of xyz frame in Fig. 6. Although in equilibrium state, this pattern is unstable, as it may

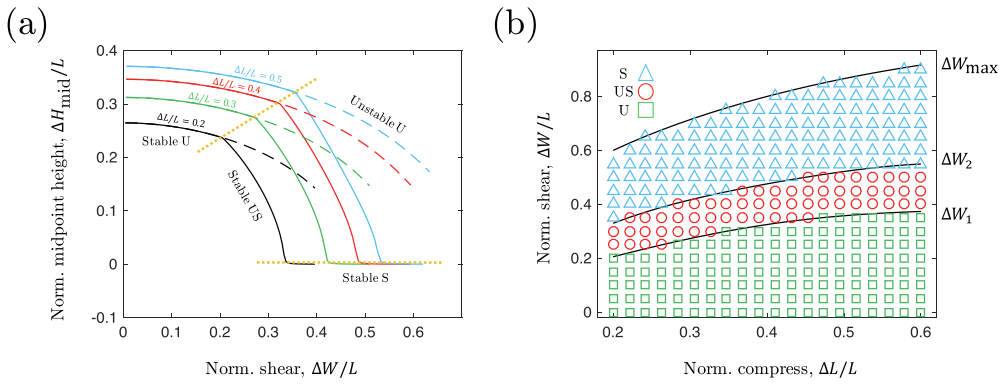

Fig. 3. (a) Relations between the normalized midpoint height, $\Delta H_{\text{mid}}/L$, and the normalized transverse shear, $\Delta W/L$, for different pre-compressed distances, $\Delta L/L \in \{0.2, 0.3, 0.4, 0.5\}$. The threshold of transverse displacements between different categories are illustrated as dotted yellow lines. (b) Phase diagram of elastic ribbons with different boundary conditions.

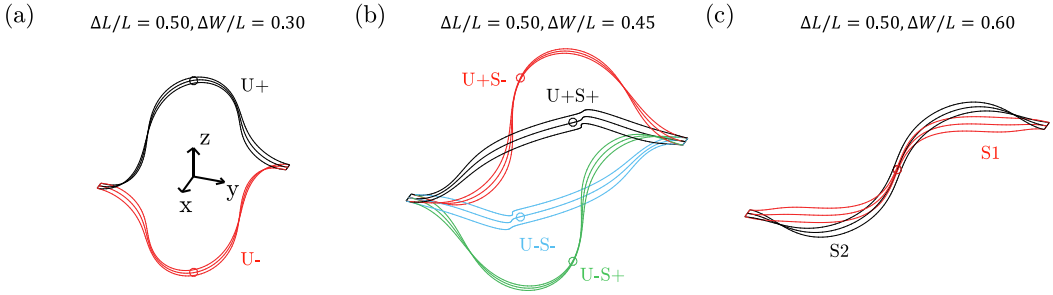

Fig. 4. Configurations of elastic ribbons in different diagrams: (a) *U* pattern, (b) *US* pattern, and (c) *S* pattern.

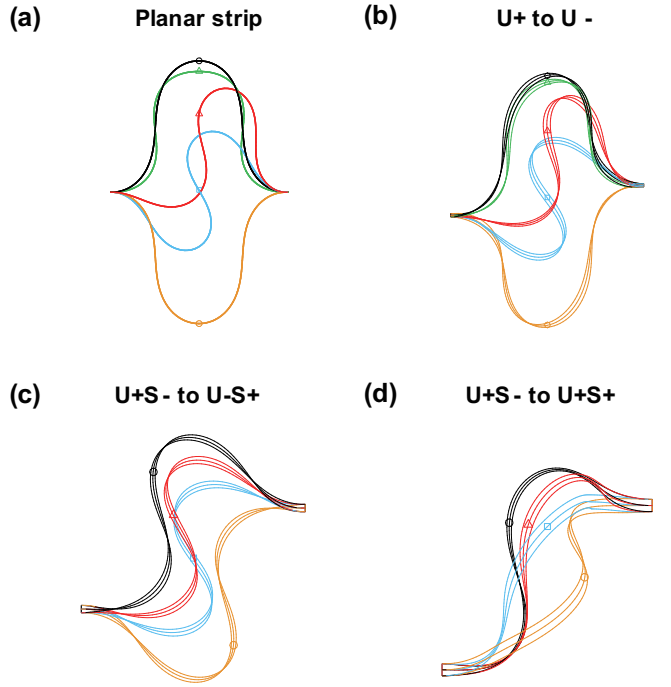

Fig. 5. Snapshots of pre-deformed ribbons during snap-through processes. (a) Planar case. (b) From *U+* to *U−*. (c) From *U+S−* to *U−S+*. (d) From *U+S−* to *U+S+*. The definitions and configurations can be found in Fig. 4. Here, the midpoints are highlighted by markers. See Movie S1 for a detailed procedure.

transform to *U+* (or *U−*) once the restriction on the structural midpoint is released.

It becomes more complex when the transverse shear is introduced and the problem is in 3D. Similar to the 2D case discussed before, the ribbon stays as a symmetric *U* diagram if the transverse displacement is smaller than the first supercritical pitchfork bifurcation point, ΔW_1. The maximum vertical force (as well as compressive strain) that induces the supercritical pitchfork bifurcation, not so surprisingly, shows a declined tendency as the transverse shear increases. e.g., the threshold of vertical displacement for $\Delta W/L = 0.3$ is $\bar{\delta} \approx 0.02$, slightly smaller compared with the 2D bistable beam. Interestingly, if the transverse shear is very close to the first threshold, ΔW_1, the peak in force–displacement curve disappears and the external force remains almost unchanged within a certain range. Dependency of the maximum external force on the transverse shear is illustrated in Fig. 7(b). A dramatic variation of the maximum force with respect to the transverse shear can be found when the value of the transverse shear is close to the first threshold, ΔW_1.

Once the transverse displacement exceeds the first critical value, ΔW_1, the structural symmetry fails to maintain, and, as a result, its midpoint doesn't locate on the *z* axis. It is obvious that there are four stable configurations with this prescribed boundary condition, and each of them may switch to another one when external actuations are imposed on the midpoint. Fig. 8(a1) and (b1) show the snap-through process between *U+S+* and *U−S−*. Similar to the previous *U* circumstance, the midpoints of the two stable patterns are symmetric to the origin point. However, the

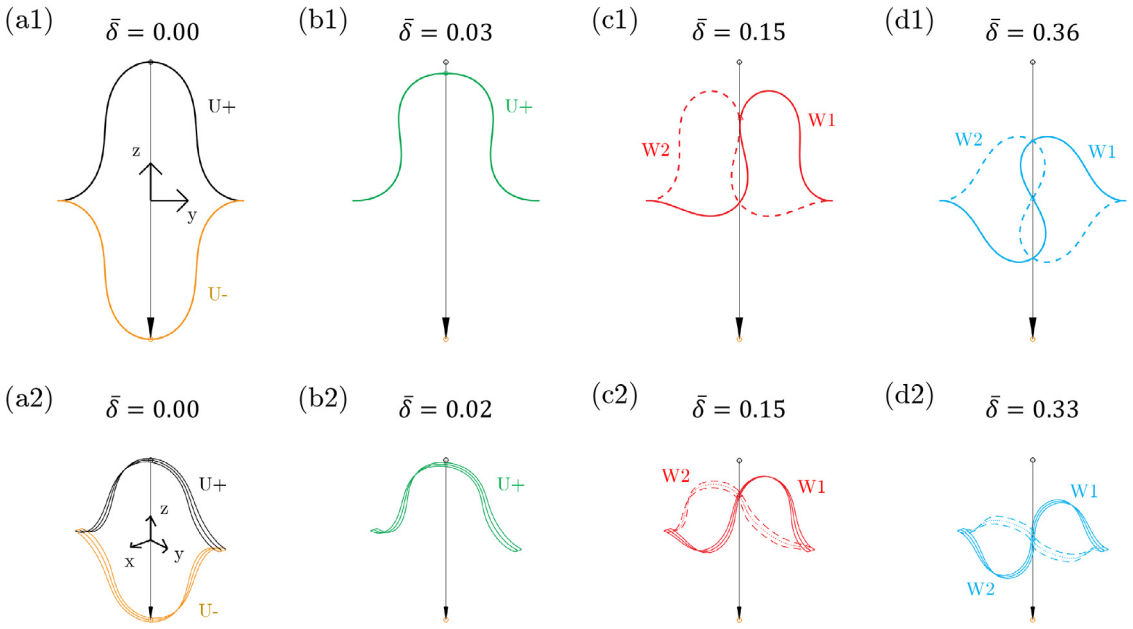

Fig. 6. Snap-through buckling in symmetric *U* pattern. (a1)–(d1) Planar case, $\Delta W/L = 0.0$. (a2)–(d2) 3D case, $\Delta W/L = 0.3$.

supercritical pitchfork bifurcation observed in the snap-through process of a symmetric *U* pattern vanishes in the unsymmetric *US* configuration, as it has already happened during the transverse shearing. With the ribbon center constrained at the original point, an unstable *S* pattern is found as it is also in equilibrium. Also, unlike the snap-through process of *U* case that *W*1 can easily switch to *W*2 under small disturbances, *S*1 can only be derived from *U*+*S*+ and *U*−*S*−, and *S*2 can only be obtained from *U*+*S*− and $U-S+$; *S*1 cannot deform to *S*2 without partial flipping or introducing stretching energies to ribbon centerline. For example, *S*1 could deform into *S*2 if a twist is applied onto the middle region of the ribbon. Here, the names *S*1 and *S*2 are arbitrarily chosen, i.e., we name the intermediate pattern between *U*+*S*+ and *U*−*S*− as *S*1, and the one between *U*+*S*− and *U*−*S*+ is called *S*2. The required snap-through actuation, similarly, has a decreased trend over the transverse shear as shown in Fig. 9(a1) and (b1).

As there are more than two stable configurations in *US* diagram, some other snap-through processes may exist in this simple structure and naive boundary setup. Fig. 8(a2) and (b2) illustrate the trajectory of the ribbon midpoint during the snap-through approach between *U*+*S*+ and *U*+*S*− (as well as between *U*−*S*+ and *U*−*S*−), and the intermediate equilibrium but unstable phase is *U*+ (as well as *U*−). The target position of midpoint for the unstable *U* pattern is indicated by the dashed line in Fig. 3a1). Several representative configurations can be found in Fig. 8(a2) and (b2). Moreover, in contrast to the snap-through process between *U*+*S*+ and *U*−*S*−, it was found that the maximal loading force in this procedure showed an reverse trend, i.e., it would increase as the growth of transverse shear, referring to Fig. 9(b2).

Interestingly, the snap-through process between *U*+*S*− and *U*−*S*− (similar for *U*+*S*+ and *U*−*S*+) is impossible to achieve via moving the midpoint directly, since *U*+*S*− and *U*−*S*− are not symmetric about the $x-y$ plane, i.e., constraining the midpoints of *U*+*S*− and *U*−*S*− to $x-y$ plane is neither overlapped nor under equilibrium, referring to Fig. 8(a3) and (b3) for details. The snap-through behavior is not found between the *S*1 and the *S*2

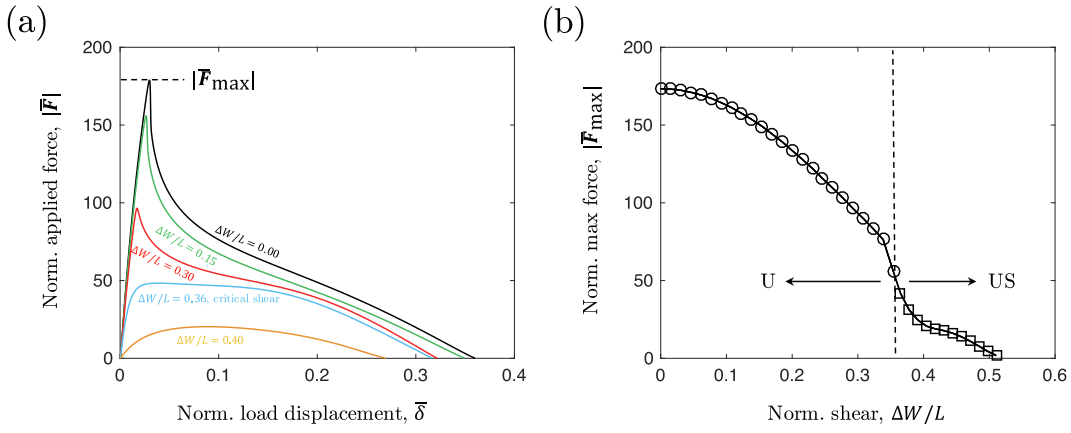

Fig. 7. (a) Normalized external force, $|\bar{\mathbf{F}}|$, as a function of normalized midpoint displacements, $\bar{\delta}$, from *U*+ (and *U*+*S*+) to *U*− (and *U*−*S*−) progress, with different transverse shear, $\Delta W/L \in \{0.00, 0.15, 0.30, 0.36, 0.40\}$. (b) Normalized maximum external force, $|\bar{\mathbf{F}}_{\max}|$, as a function of normalized transverse shear, $\Delta W/L$. Here the pre-compressed distance is fixed as $\Delta L/L = 0.5$.

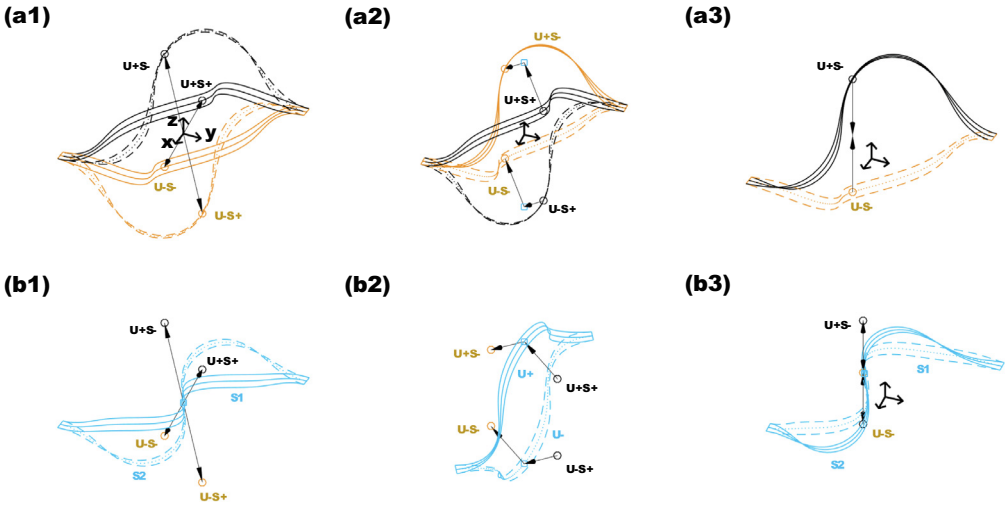

Fig. 8. Configurations of elastic ribbons during the snap-through procedure. (a1)–(b1) The path between U+S+ and $U-S-$ (solid lines) as well as between U+$S-$ and $U-S$+ process (dashed lines). (a2)–(b2) The path between U+S+ and U+$S-$ (solid lines) as well as between $U-S$+ and $U-S-$ process (dashed lines). (a3)–(b3) Failure of the transformation between U+$S-$ and $U-S-$. Here the pre-compressed distance and the transverse shear are fixed as $\Delta L/L = 0.5$and $\Delta W/L = 0.45$, separately.

configurations, e.g., if a twist is imposed onto the structural middle, partial flip will happen and a quite large stretching energy is required between the switch of the two S patterns.

Thus far, we fix the pre-compressed distance at $\Delta L/L = 0.5$. Exploiting the efficiency and robustness of DDG-based simulators, a two dimensional parameter sweep is performed by varying the pre-compressed distance and the transverse shear, to show the variation of the maximal actuating force, $|\bar{\mathbf{F}}_{\max}|$. As illustrated in Fig. 10(a), the normalized maximal external force, $|\bar{\mathbf{F}}_{\max}|$, acts as a function of the pre-compressed strain, $\Delta L/L$, and the transverse

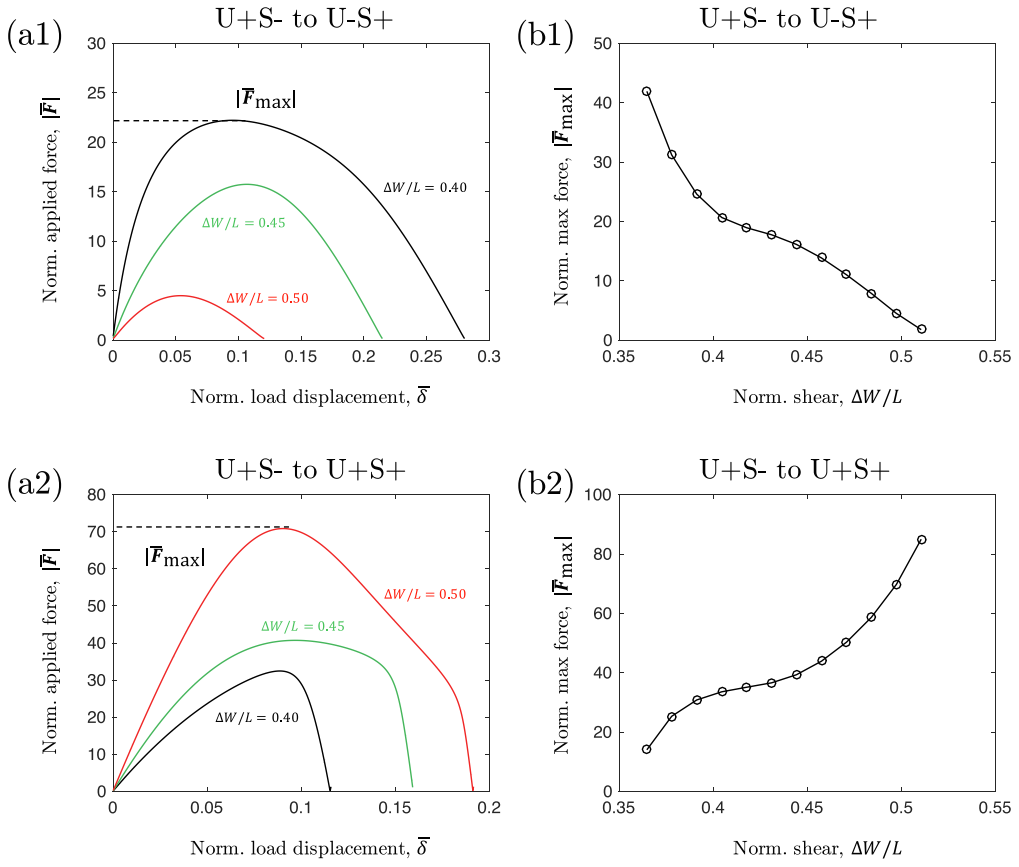

Fig. 9. Normalized external force, $|\bar{\mathbf{F}}|$, as a function of normalized midpoint displacements, $\bar{\delta}$ in (a1) U+$S-$ (and U+S+) to $U-S$+ (and $U-S-$) process and (a2) U+$S-$ (and $U-S$+) to U+S+ (and $U-S-$) process. Relations between the normalized maximum external force, $|\bar{\mathbf{F}}_{\max}|$, and the normalized transverse shear, $\Delta W/L$ for (b1) U+$S-$ (and U+S+) to $U-S$+ (and $U-S-$) process and (b2) U+$S-$ (and $U-S$+) to U+S+ (and $U-S-$) process.

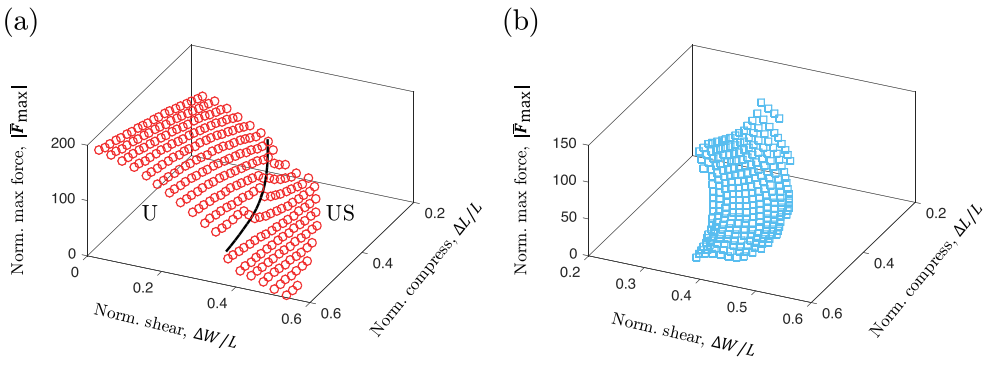

Fig. 10. Normalized maximum external force, $|\bar{\mathbf{F}}_{max}|$, as a function of normalized pre-compressed distance, $\Delta L/L$, and normalized transverse shear, $\Delta W/L$, for different snap-through procedures. (a) From *U*+ (and $U+S\pm$) to *U*− (and $U-S\pm$). The boundary between *U* and *US* patterns is highlighted by solid black line. (b) From *U*+*S*− (and *U*−*S*+) to *U*+*S*+ (and *U*−*S*−).

motion, $\Delta W/L$, during the snap-through process between *U*+ and *U*− (as well as between *U*+*S*+ and *U*−*S*−). The required force increases with respect to the pre-compressed distance, while a reverse trend is found with respect to the transverse shear. In addition, the boundary between *U* and *US* patterns can be clearly observed – the point at which the actuating force drops dramatically. The relations between the maximal external force and the two distances for the snap-through between *U*+*S*+ and *U*+*S*− (as well as between *U*−*S*+ and *U*−*S*−) are in Fig. 10(b), which exhibits an reverse tendency compared with the previous procedure.

5. Conclusion

We numerically explored the snap-through buckling behaviors of elastic ribbons subjected to compression, shear, and movement of the midpoint. A discrete model was derived from the anisotropic Kirchhoff rod theory, which could address the geometrically nonlinear deformation of a narrow ribbon. The pre-buckled elastic ribbons would transform to several (anti) symmetric patterns when the transverse shear was applied, and one pattern might switch to another if its midpoint was actuated moving along a prescribed path. As expected, the snap-through buckling behavior found in the symmetric *U* configuration showed a similar procedure to the well-established bisTable 2D beam. Meanwhile, two novel snap-through phenomena were observed in the bifurcate *US* diagram, some of which, however, could not be converted to others without partial flipping unless a relatively large stretching energy was introduced to the inextensible rod system. Finally, the maximal actuation force that was required to produce different deformed patterns and various snap-through procedures were illustrated via a quick search implementation through a thorough parameter sweeping. In the future, we plan to investigate the flipping behaviors between *U*+*S*− and *U*−*S*− (as well as *U*+*S*+ and *U*−*S*+) configurations with a more general 1D ribbon model formulated in Ref. Sano and Wada (2019) and Audoly and Neukirch (xxxx). As found in this paper, sudden jump or unexpected transformations may occur during the snap-through process, which could be applied as driving force for soft robots or utilized to avoid unwanted behaviors when an elastic ribbon-like structure is manipulated, which, we hope, could inspire the designs of soft robots and functional materials.

Declaration of Competing Interest

The authors declare that they have no known competing financial interests or personal relationships that could have appeared to influence the work reported in this paper.

Acknowledgements

This work was supported by the Fundamental Research Funds for the Central Universities (No. 2242021R10024).

Appendix A. Supplementary data

Supplementary data associated with this article can be found, in the online version, at https://doi.org/10.1016/j.ijsolstr.2021.111184.

References

Ameline, O., Haliyo, S., Huang, X., Cognet, J.A., 2017. Classifications of ideal 3d elastica shapes at equilibrium. Journal of Mathematical Physics 58, (6) 062902.
Antman, S.S., Jordan, K.B., 1975. 5. – Qualitative aspects of the spatial deformation of non-linearly elastic rods. Proceedings of the Royal Society of Edinburgh Section A: Mathematics 73, 85–105..
Antman, S.S., Kenney, C.S., 1981. Large buckled states of nonlinearly elastic rods under torsion, thrust, and gravity. Archive for Rational Mechanics and Analysis 76 (4), 289–338.
Audoly, B., Neukirch, S. A one-dimensional model for elastic ribbons: a little stretching makes a big difference..
Bergou, M., Wardetzky, M., Robinson, S., Audoly, B., Grinspun, E., 2008. Discrete elastic rods. In: ACM Transactions on Graphics (TOG), vol. 27, ACM, p. 63..
Bergou, M., Audoly, B., Vouga, E., Wardetzky, M., Grinspun, E., 2010. Discrete viscous threads. In: ACM Transactions on Graphics (TOG), vol. 29, ACM, p. 116..
Bertoldi, K., Vitelli, V., Christensen, J., van Hecke, M., 2017. Flexible mechanical metamaterials. Nature Reviews Materials 2 (11), 17066.
Bonet, J., Wood, R.D., 1997. Nonlinear Continuum Mechanics for Finite Element Analysis. Cambridge University Press.
Camescasse, B., Fernandes, A., Pouget, J., 2013. Bistable buckled beam: Elastica modeling and analysis of static actuation. International Journal of Solids and Structures 50 (19), 2881–2893.
Camescasse, B., Fernandes, A., Pouget, J., 2014. Bistable buckled beam and force actuation: Experimental validations. International Journal of Solids and Structures 51 (9), 1750–1757.
Cazzolli, A., Dal Corso, F., 2019. Snapping of elastic strips with controlled ends. International Journal of Solids and Structures 162, 285–303.
Chen, J.-S., Hua, L.-Y., 2018. Effects of clamping misalignments on the line-contact deformation of a constrained elastica. International Journal of Non-Linear Mechanics 99, 288–294.
Chen, T., Bilal, O.R., Shea, K., Daraio, C., 2018. Harnessing bistability for directional propulsion of soft, untethered robots. Proceedings of the National Academy of Sciences 115 (22), 5698–5702.
Chen, T., Pauly, M., Reis, P.M., 2021. A reprogrammable mechanical metamaterial with stable memory. Nature 589 (7842), 386–390.
De Borst, R., Crisfield, M.A., Remmers, J.J., Verhoosel, C.V., 2012. Nonlinear Finite Element Analysis of Solids and Structures. John Wiley & Sons.
Doedel, E.J., 2007. Lecture notes on numerical analysis of nonlinear equations. In: Numerical Continuation Methods for Dynamical Systems, Springer, pp. 1–49..
Faris, W., Nayfeh, A.H., 2007. Mechanical response of a capacitive microsensor under thermal load. Communications in Nonlinear Science and Numerical Simulation 12 (5), 776–783.
Forterre, Y., Skotheim, J.M., Dumais, J., Mahadevan, L., 2005. How the venus flytrap snaps. Nature 433 (7024), 421.

Gomez, M., Moulton, D.E., Vella, D., 2017. Critical slowing down in purely elastic snap-through instabilities. Nature Physics 13 (2), 142.
Goyal, S., Perkins, N.C., Lee, C.L., 2005. Nonlinear dynamics and loop formation in kirchhoff rods with implications to the mechanics of dna and cables. Journal of Computational Physics 209 (1), 371–389.
Grinspun, E., Desbrun, M., Polthier, K., Schröder, P., Stern, A., 2006. Discrete differential geometry: an applied introduction. ACM SIGGRAPH Course 7, 1–139.
Hu, N., Burgueño, R., 2015. Buckling-induced smart applications: recent advances and trends. Smart Materials and Structures 24, (6) 063001.
Huang, W., Wang, Y., Li, X., Jawed, M.K., 2020. Shear induced supercritical pitchfork bifurcation of pre-buckled bands, from narrow strips to wide plates. Journal of the Mechanics and Physics of Solids 145, 104168.
Hughes, T.J., 2012. The Finite Element Method: Linear Static and Dynamic Finite Element Analysis. Courier Corporation..
Jawed, M.K., Da, F., Joo, J., Grinspun, E., Reis, P.M., 2014. Coiling of elastic rods on rigid substrates. Proceedings of the National Academy of Sciences 111 (41), 14663–14668.
Kebadze, E., Guest, S., Pellegrino, S., 2004. Bistable prestressed shell structures. International Journal of Solids and Structures 41 (11–12), 2801–2820.
Kehrbaum, S., Maddocks, J., 1999. Elastic rods, rigid bodies, quaternions and the last quadrature. In: Localization And Solitary Waves In Solid Mechanics, World Scientific, pp. 181–200..
Kodio, O., Goriely, A., Vella, D., 2020. Dynamic buckling of an inextensible elastic ring: Linear and nonlinear analyses. Physical Review E 101, (5) 053002.
Liu, Y., Wang, X., Xu, Y., Xue, Z., Zhang, Y., Ning, X., Cheng, X., Xue, Y., Lu, D., Zhang, Q., et al., 2019. Harnessing the interface mechanics of hard films and soft substrates for 3d assembly by controlled buckling. Proceedings of the National Academy of Sciences 116 (31), 15368–15377.
Liu, M., Gomez, M., Vella, D., 2021. Delayed bifurcation in elastic snap-through instabilities. Journal of the Mechanics and Physics of Solids 104386.
Morigaki, Y., Wada, H., Tanaka, Y., 2016. Stretching an elastic loop: Crease, helicoid, and pop out. Physical Review Letters 117, (19) 198003.
Nizette, M., Goriely, A., 1999. Towards a classification of euler–kirchhoff filaments. Journal of Mathematical Physics 40 (6), 2830–2866.
Pandey, A., Moulton, D.E., Vella, D., Holmes, D.P., 2014. Dynamics of snapping beams and jumping poppers. EPL (Europhysics Letters) 105 (2), 24001.
Sadowsky, M., 1930. Ein elementarer Beweis für die Existenz eines abwickelbaren Möbiusschen Bandes und Zurückführung des geometrischen Problems auf ein Variationsproblem..
Sano, T.G., Wada, H., 2018. Snap-buckling in asymmetrically constrained elastic strips. Physical Review E 97, (1) 013002.
Sano, T.G., Wada, H., 2019. Twist-induced snapping in a bent elastic rod and ribbon. Physical Review Letters 122, (11) 114301.
Tang, Y., Chi, Y., Sun, J., Huang, T.-H., Maghsoudi, O.H., Spence, A., Zhao, J., Su, H., Yin, J., 2020. Leveraging elastic instabilities for amplified performance: Spine-inspired high-speed and high-force soft robots. Science Advances 6 (19), eaaz6912.
Wan, G., Liu, Y., Xu, Z., Jin, C., Dong, L., Han, X., Zhang, J.X., Chen, Z., 2019. Tunable bistability of a clamped elastic beam. Extreme Mechanics Letters 100603.
Wood, R.D., Zienkiewicz, O., 1977. Geometrically nonlinear finite element analysis of beams, frames, arches and axisymmetric shells. Computers & Structures 7 (6), 725–735.
Wunderlich, W., 1962. Über ein abwickelbares möbiusband. Monatshefte für Mathematik 66 (3), 276–289.
Yan, W., Yu, Y., Mehta, A., 2019. Analytical modeling for rapid design of bistable buckled beams. Theoretical and Applied Mechanics Letters 9 (4), 264–272.
Yu, T., Hanna, J., 2019. Bifurcations of buckled, clamped anisotropic rods and thin bands under lateral end translations. Journal of the Mechanics and Physics of Solids 122, 657–685.
Zhang, Y., Jiao, Y., Wu, J., Ma, Y., Feng, X., 2019. Configurations evolution of a buckled ribbon in response to out-of-plane loading. Extreme Mechanics Letters 100604.
Zhao, J., Jia, J., He, X., Wang, H. Post-buckling and snap-through behavior of inclined slender beams, Journal of Applied Mechanics 75 (4)..
Zienkiewicz, O.C., Taylor, R.L., 2005. The Finite Element Method for Solid and Structural Mechanics. Elsevier.